HAL open science

SpliceAI-visual: a free online tool to improve SpliceAI splicing variant interpretation

Jean-Madeleine de Sainte Agathe, Mathilde Filser, Bertrand Isidor, Thomas Besnard, Paul Gueguen, Aurélien Perrin, Charles van Goethem, Camille Verebi, Marion Masingue, John Rendu, et al.

To cite this version:

Jean-Madeleine de Sainte Agathe, Mathilde Filser, Bertrand Isidor, Thomas Besnard, Paul Gueguen, et al.. SpliceAI-visual: a free online tool to improve SpliceAI splicing variant interpretation. Human Genomics, 2023, 17 (1), pp.7. 10.1186/s40246-023-00451-1 . hal-03984779

HAL Id: hal-03984779

https://hal.science/hal-03984779v1

Submitted on 14 Feb 2023

HAL is a multi-disciplinary open access archive for the deposit and dissemination of scientific research documents, whether they are published or not. The documents may come from teaching and research institutions in France or abroad, or from public or private research centers.

L'archive ouverte pluridisciplinaire **HAL**, est destinée au dépôt et à la diffusion de documents scientifiques de niveau recherche, publiés ou non, émanant des établissements d'enseignement et de recherche français ou étrangers, des laboratoires publics ou privés.

Distributed under a Creative Commons Attribution 4.0 International License

SpliceAI-visual: a free online tool to improve SpliceAI splicing variant interpretation

Jean-Madeleine de Sainte Agathe[1,2*], Mathilde Filser[1], Bertrand Isidor[3], Thomas Besnard[3], Paul Gueguen[2,4], Aurelien Perrin[5], Charles Van Goethem[5], Camille Verebi[6], Marion Masingue[7], John Rendu[8], Mireille Cossee[5,9], Anne Bergougnoux[5,9], Laurent Frobert[2], Julien Buratti[1], Elodie Lejeune[1], Eric Le Guern[1,2], Florence Pasquier[10], Fabienne Clot[1], Vasiliki Kalatzis[11], Anne Francoise Roux[5,12], Benjamin Cogne[2,3] and David Baux[5,12]

1 Departement de Genetique Medicale, Groupe Hospitalier Universitaire de la Pitie Salpetriere, AP-HP.Sorbonne Universite, Laboratoire de Medecine Genomique Sorbonne Universite, Paris, France.

2 Laboratoire de Biologie Medicale Multi-Sites SeqOIA (laboratoire-seqoia.fr/), Paris, France.

3 Nantes Universite, CHU Nantes, Service de Genetique Medicale, 44000 Nantes, France.

4 Service de Genetique, Inserm U1253, CHRU de Tours, Tours, France.

5 Laboratoire de Genetique Moleculaire, CHU de Montpellier, Universite de Montpellier, Montpellier, France.

6 Service de Medecine Genomique, Maladies de Système et d'Organe, Federation de Genetique et de Medecine Genomique, DMU BioPhyGen, APHP Centre-Universite Paris Cite, Hopital Cochin, Paris, France.

7 Centre de reference des maladies neuromusculaires Nord/Est/Ile de France, Hopital Pitie-Salpetriere, APHP, Paris, France.

8 Inserm, U1216, CHU Grenoble Alpes, Grenoble Institut Neurosciences, Universite Grenoble Alpes, Grenoble, France.

9 PhyMedExp, INSERM, CNRS, Universite de Montpellier, Montpellier, France.

10 Centre memoire, Inserm U1172 DistALZ, Licend, Univ Lille, CHU Lille, 59000 Lille, France.

11 INM, Univ Montpellier, INSERM, Montpellier, France.

12 INM, Univ Montpellier, INSERM, CHU Montpellier, Montpellier, France.

***Correspondence:**

Jean-Madeleine de Sainte Agathe jean-madeleine.desainteagathe@aphp.fr

Abbreviations

ACMG American College of Medical Genetics and Genomics; AG Acceptor gain; AL Acceptor loss; DG Delta gain; DL Delta loss; DS Delta score; BAM Binary Alignment Map OMIM Online Mendelian Inheritance in Man; RS Raw score; RT-PCR Reverse transcription-polymerase chain reaction; PVS1 ACMG evidence of Pathogenicity with Very Strong weight-1.

Abstract

SpliceAI is an open-source deep learning splicing prediction algorithm that has demonstrated in the past few years its high ability to predict splicing defects caused by DNA variations. However, its outputs present several drawbacks: (1) although the numerical values are very convenient for batch filtering, their precise interpretation can be difficult, (2) the outputs are delta scores which can sometimes mask a severe consequence, and (3) complex delins are most often not handled. We present here SpliceAI-visual, a free online tool based on the SpliceAI algorithm, and show how it complements the traditional SpliceAI analysis. First, SpliceAI-visual manipulates raw scores and not delta scores, as the latter can be misleading in certain circumstances. Second, the outcome of SpliceAI-visual is user-friendly thanks to the graphical presentation. Third, SpliceAI-visual is currently one of the only SpliceAI-derived implementations able to annotate complex variants (e.g., complex delins). We report here the benefits of using SpliceAI-visual and demonstrate its relevance in the assessment/modulation of the PVS1 classification criteria. We also show how SpliceAI-visual can elucidate several complex splicing defects taken from the literature but also from unpublished cases. SpliceAI-visual is available as a Google Colab notebook and has also been fully integrated in a free online variant interpretation tool, MobiDetails (https:// mobid etails. iurc. montp. inserm. fr/ MD).

Introduction

Exome and genome sequencing currently identify on a daily basis many novel or uncharacterized variants worldwide. A significant proportion (up to 60% [1]) of the pathogenic variants identified are likely to alter the correct splicing of the transcript. However, the functional validation of a variant predicted to alter splicing requires in vitro tests or additional and sometimes invasive biological samples. These validations are often time-consuming and expensive. Therefore, there is a strong need for in silico tools that can facilitate the precise interpretation of candidate variants to (1) correctly prioritize the best candidates to be investigated, and (2) choose the optimal functional validation test according to the expected alteration. The efficiency of SpliceAI to predict a variant's splicing alteration has been attested by multiple studies [2–10]. Furthermore, thanks to its neural network, SpliceAI is able to make predictions about the global splicing outcome (e.g., exon skipping, splicing rescue by cryptic site activation, pseudo-exon creation, etc.). This ability to focus not only on the nearby site (destruction or creation) but at the whole transcript level is a unique feature of these deep-learning-based next-generation splicing predictors, such as SpliceAI or Pangolin [11]. In a recent improvement, the SpliceAI neural network has been retrained with a curated and manually validated isoforms dataset [12]. Still, the standard version of SpliceAI

(currently v1.3.1) has some limitations. First, predictions and relative positions of the altered splice sites are displayed as numerical values, which can be confusing when estimating which exact sites are altered, or when dealing with long-distance effects. Second, the results are the delta scores (DS) between the raw scores (RS) of the reference allele and the variant allele, which can be difficult to interpret and in some cases misleading, in particular when the reference value is comprised within the intermediate range of interpretation (i.e., [0.2–0.8]). Indeed, the DS provided by the genuine SpliceAI account for the maximal differences between the predictions of the variant and the reference allele, for the 4 predicted categories being acceptor gain (AG), acceptor loss (AL), donor gain (DG), and donor loss (DL). In the original publication describing SpliceAI, the DS cutoff of 0.2 has been characterized as a "permissive" threshold to retain splice altering variants with high sensitivity [2]. Therefore, this threshold is widely used, but may filter out pathogenic variants if the difference is subtle (i.e., increase in an already high donor or acceptor site). Finally, SpliceAI current public implementations (e.g., splice ailo okup, https:// splic eailo okup. broad insti tute. org/) or pre-computed whole genome VCFs only annotate simple variants (i.e., substitutions, insertions, deletions), prohibiting the interpretation of more complex deletions–insertions or inversions, with the notable exception of the recent CISpliceAI [12].

To overcome these limitations, we developed SpliceAI visual, a simple and free-to-use online tool, based on the original SpliceAI model, which provides the SpliceAI's RS. Available via a Google Colab notebook (https://tinyu rl. com/ splic eai- visual), the SpliceAI-visual predictions are graphically displayed on a dynamic window, and bed Graph files are downloadable for further analyses in a standard genome browser (compatible with IGV and UCSC Genome Browser) [13, 14]. In addition, the SpliceAI-visual solution has been implemented in Mobi-Details (https:// mobid etails. iurc. montp. inserm. fr/ MD), a free online user-friendly DNA variant interpretation tool, and is displayed by default for any annotated variant [15]. Here, we validated the advantage of using SpliceAI visual on variants from the literature and we show how it helped to identify new splicing-altering variants, to reconsider the loss-of-function prediction (i.e., modulating PVS1), and to interpret complex variants.

Methods

In this study, we refer to "raw" scores (RS) for the absolute prediction of SpliceAI, in opposition to the "delta" scores (DS). We wish to dismiss any confusion concerning the "raw" scores found in the SpliceAI terminology, referring there to "raw" delta scores, in opposition to "masked" delta scores (see https:// github. com/ Illum ina/ Splic eAI for more details).

SpliceAI‑visual

For SpliceAI-visual, the SpliceAI model (https:// github.com/ Illum ina/ Splic eAI, custom sequence function) is run independently on two sequences (reference allele; variant allele), generating for each nucleotide its likelihood (RS) to be used as an acceptor or a donor site in a biological context. Results are then used to generate 2 bedGraph files (http:// genome. ucsc. edu/ golde nPath/help/ bedgr aph. html). In the Colab notebook, scores are computed for both the entire reference and variant transcripts in real time. The reference and variant bedGraph files can be loaded in a genome browser.

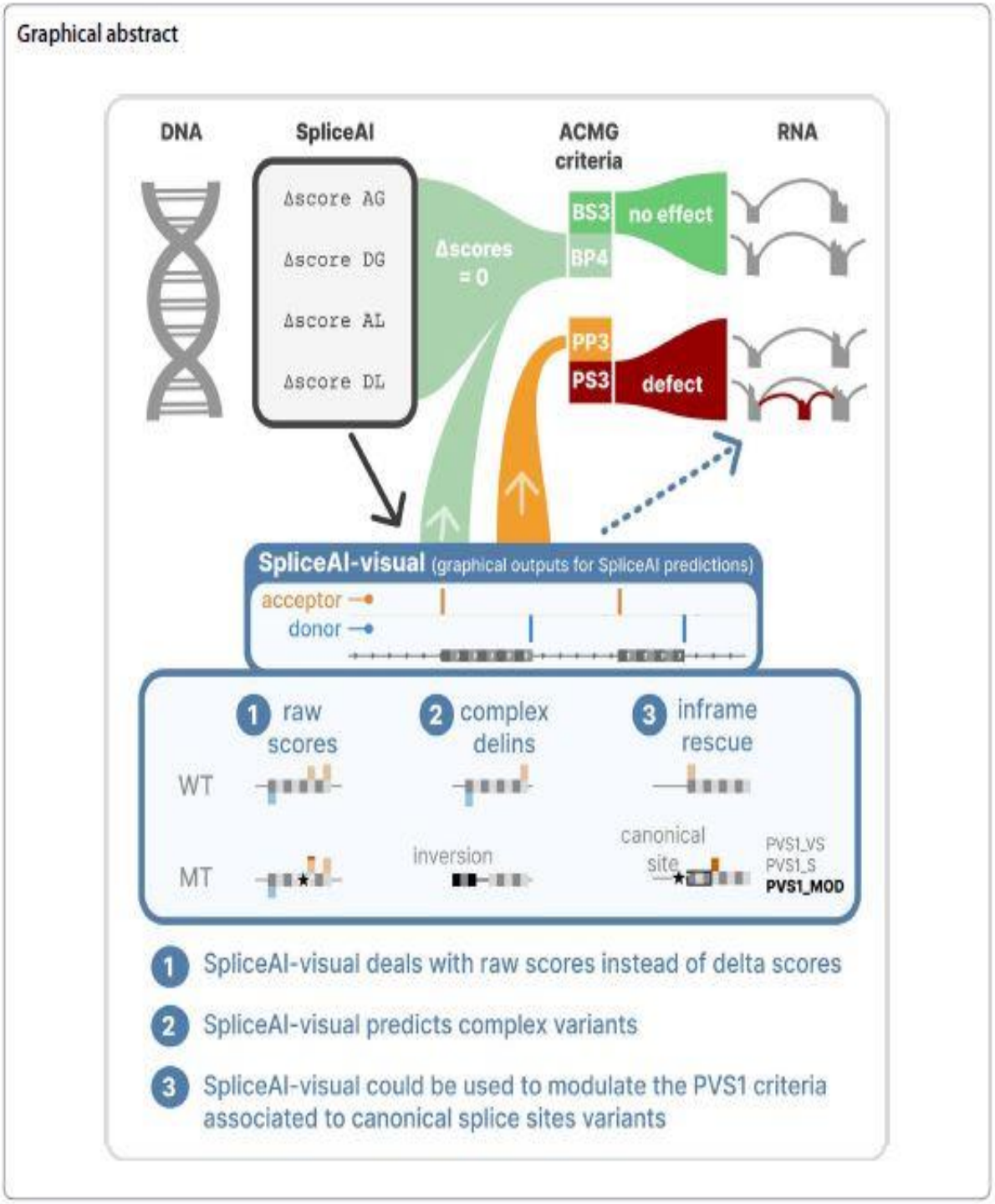

To integrate SpliceAI-visual in MobiDetails, we have used SpliceAI v1.3.1 to pre-compute the RS for 57,271 transcripts including 19,120 Matched Annotation by NCBI and EMBL-EBI (MANE) transcripts available on the Web site [16], using Illumina® models available for non-commercial usage (see https:// github. com/ Illum ina/Splic eAI for more details). Then, RS predictions for the wild-type sequences for these full transcripts are stored as bed Graph files and are directly available for comparison with the variant RS predictions. RS predictions for the variant have to be computed in real time (the software architecture is described in Additional file 1: Fig. S1). The variant allele consists of 10 kb of genic sequence surrounding

the variation (truncated if the variation is located less than 5 kb from the 3' or 5' end of the transcript). Indeed, the authors of SpliceAI have shown that their algorithm was the most accurate using 5 kb of DNA sequence surrounding the variant position [2]. We added an additional 5 kb on each side of the variant to display a larger picture of the splicing pattern of the region.

A dedicated Flask API (https:// palle tspro jects. com/p/ flask/) available in a private server (source code available at https:// github. com/ mobid ic/ splic eai) is asynchronously called by the public MobiDetails server to compute the variant allele RS (in about 30 s) (see Additional file 1: Fig. S1). Computation requests on the private server are handled by the Apache Web server (https:// apache. org/) and queued with the SLURM workload manager (https:// slurm. sched md. com/). SpliceAI is run in CPU-only mode. The API returns JSON objects including the DNA sequence and the associated SpliceAI RS, which are converted into Bed Graphs by the MobiDetails public server. Bed Graphs are then displayed on the Web page within an igv.js genome browser (https:// github. com/ igvte am/ igv. js/) as two separate tracks (reference and variant BedGraphs). A third track is optionally provided corresponding to the RS of the extra inserted nucleotides when the variant allele is longer than the reference allele. As an option, users can request in a simple click the prediction of the whole variant transcript, which is displayed in a dedicated track in the genome browser. In this case, the computation time directly depends on the size of the transcript (from seconds to several minutes).

SpliceAI delta scores

The SpliceAI DS of the variants explored in this study were generated using SpliceAI v1.3.1, with the maximal window of ± 4999 bp surrounding the variant on the MANE select transcript.

DNA, RNA, and plasma progranulin analysis

DNA sequencing and RNA sequencing were performed through various methods and protocols, as described in the Additional file 1: Methods. Briefly, DNA sequencing of the *SETD5* cases (patient 1 and 5) was performed by trio-based genome sequencing, DNA sequencing of patient 2 was performed by Sanger sequencing of the exons of *GRN*, DNA sequencing of patient 3 was performed by trio-based exome sequencing, DNA sequencing of patient 4 was performed by targeted gene sequencing (gene panel) and plasma progranulin levels were measured by ELISA, as described in the Additional file 1: Methods.

Results

We developed SpliceAI-visual, which displays SpliceAI's RS on a genome browser. SpliceAI-visual betterments compared to SpliceAI are summarized in Table 1.

Table 1 SpliceAI-visual solves some SpliceAI limitations

SpliceAI limitation	SpliceAI-visual enhancement
Numerical values	Graphical outputs, allowing fast and precise interpretation especially for PVS1 modulation
Delta scores pitfall	Raw scores
Complex delins not annotated	Complex delins annotated

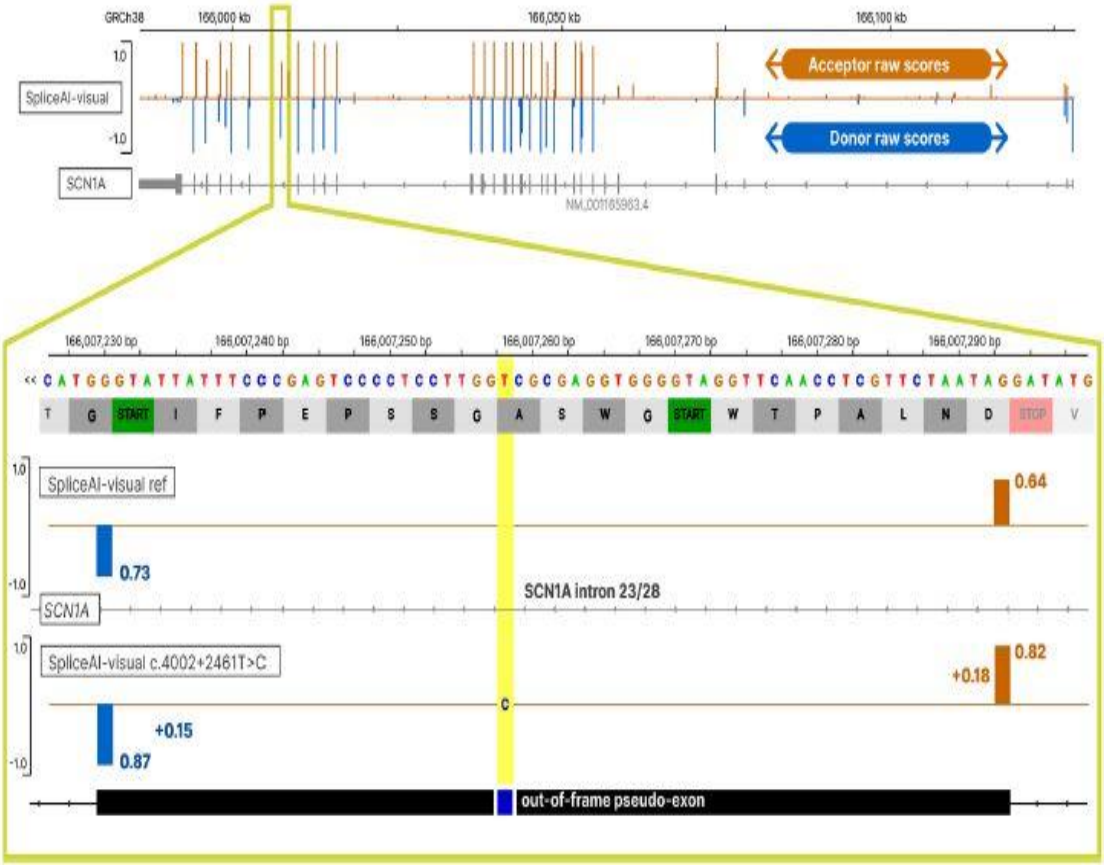

Fig. 1 The delta score (DS) pitfall: discrepancy between SpliceAI's DS and SpliceAI raw scores (RS).

SpliceAI-visual outputs of *SCN1A* deep intronic variant displayed in IGV. Above: SpliceAI raw scores for the reference allele of *SCN1A*; below: SpliceAI RS for the pathogenic deep intronic variant NM_001165963.4(SCN1A):c.4002 + 2461 T > C functionally attested to cause the retention of an intronic retention of 64pb[REF]. Orange: acceptor site prediction; Blue: donor site prediction. The variant position is highlighted in yellow

Table 2 HGVS descriptions, SpliceAI, SpliceAI-visual scores, and ACMG classification of the variants analyzed in this study

Gene symbol	Coding/protein	SpliceAI DS(DP)*	SpliceAI-visual RS(DP)**	Category/Reference	ACMG
SCN1A	NM_001165963.4:c.4002+2461 T>C p.?	AG=0.18 (35) AL=0 DG=0.15 (−28) DL=0	Ref: A=0.64 (35), D=0.73 (−28) Var: A=0.82 (35), D=0.87 (−28)	DS pitfall pseudo-exonization/Li et al., 2021	Likely pathogenic (PS3, PM2, PP1)
MFGE8	NM_005928.4:c.871-803A>G p.?	AG=0.15 (144) AL=0 DG=0.16 (43) DL=0	Ref: A=0.68 (144), D=0.58 (43) Var: A=0.84 (144), D=0.74 (43)	DS pitfall Yamaguchi et al., 2010	Not Applicable (candidate gene)
SETD5	NM_001080517.3:c.2476+198A>C p. ?	AG=0.05 (−61) AL=0 DG=0.04 (35) DL=0	Ref: A=0.94 (−61), D=0.96 (35) Var: A=0.99 (−61), D=0.99 (35)	DS pitfall This study	Pathogenic (PS3, PS2, PM2)
GRN	NM_002087.4:c.-9A>G p.?	AG=0 AL=0 DG=0.19 (272) DL=0.48 (1)	Ref: D=0.94 (1) Var: D=0.44 (1)	DS pitfall This study	Likely pathogenic (PS3, PP5, PM2, PP4)
CASK	NM_001367721.1:c.172+1G>A p. ?	AG=0 AL=0 DG=0.71 (−17) DL=0.99 (1)	Ref: D=0 (1), D=0.29 (−17) Var: D=0 (1), D=0.99 (−17)	Adjusting PVS1 Intronic retention of 18 bp leading to the in-frame insertion of 6 amino acids r.172_173ins[172+1_172+18] p.(Asp58delinsGlyLysArgTrpIleSerAsn) This study	Uncertain significance (PVS1_M, PM2)
KMT2D	NM_003482.4:c.5189-1G>C p.?	AL=0.98 (−1) DL=0 AG=0.95 (−25) DG=0.07 (−253)	Ref: A=1 (1), A=0.04 (−25) Var: A=0.02 (1), A=0.99 (−25)	Adjusting PVS1 11 individuals in UK Biobank exomes, prediction of the in-frame deletion of 8 amino acids	Uncertain significance (PVS1_M, PP5, BS2)
	NM_003482.4:c.5782+1G>A p.?	AL=0 DL=1 (1) AG=0.01 (−431) DG=0.28 (−8)	Ref: D=1 (1), D=0.71 (−8) Var: D=0 (1), D=1 (−8)	Adjusting PVS1 3 heterozygous individuals in gnomAD, prediction of the in-frame insertion of 3 amino acids	Uncertain significance (PVS1_M, PP5, BS2)
TTN	NM_001267550.2:c.31349-1G>C p. ?	AG=0.51 (−10) AL=0.97 (−1) DG=0 (43) DL=0 (1)	Ref: A=0.97 (−1), A=0.02 (−10), D=0.99 (−78) Var: A=0 (−1), A=0,53 (−10), D=0.80 (−78)	Adjusting PVS1 In-frame rescue acceptor site, leading to the loss of 9 bp This study	Uncertain significance (PVS1_M, PM2)
SETD5	NM_001080517.3:c.568-31_568dup p.(Asn190Ilefs*20)	AG=0.07 (0) AL=0.01 (−3574) DG=0 DL=0.01 (135)	Ref: A=0.99 (31), D=0.98 (278) Var: A=0.99 (31), D=0.98 (278)	Adjusting PVS1 This study	Benign (PM2, BS3, BS4) *Of note, PVS1 has been excluded*
EYS	NM_001142800.2:c.2992_2992+6delinsTG p.?	Not supported	Ref: A=0.97 (151), D=0.99 (6) Var: A=0.13 (151), D=0 (6)	Complex delins Westin et al. 2021	Likely pathogenic (PS3, PM2, PM3)

*SpliceAI: delta score (DS), delta position (DP), acceptor gain (AG), acceptor loss (AL), donor gain (DG), donor loss (DL)

**SpliceAI-visual: Raw scores (RS), delta position (DP) for acceptor A(DP) or donor D(DP) sites, for reference (Ref) and variant (Var) alleles

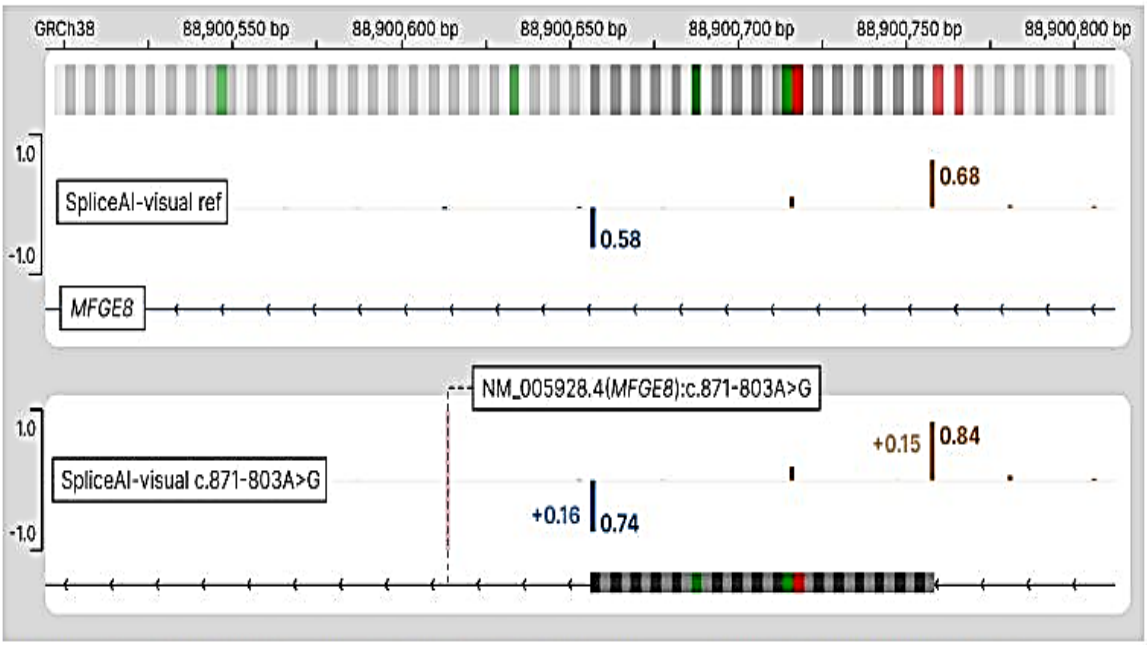

Fig. 2 The delta score (DS) pitfall: discrepancy between SpliceAI's DS and SpliceAI raw scores (RS). SpliceAI-visual outputs of *MFGE8* deep intronic variant displayed in IGV. Above: SpliceAI RS for the reference allele of *MFGE8*; below: SpliceAI RS for the pathogenic variant NM_005928.4(*MFGE8*):c.871-803A > G functionally attested to cause the exonization of an intronic sequence containing a stop codon (red). Orange: acceptor site prediction; Blue: donor site prediction. The variant position is pointed by a dashed line

Overcoming the DS pitfall

As already stated, the value of 0.2 is recommended by the authors of SpliceAI as a threshold for the four DS to discriminate potential splice-altering variants from non-altering variants. We present several examples demonstrating the relevance of SpliceAI-visual when the DS are low.

Examples from the literature

Identifying pseudo -exon inclusion

SCN1A The deep intronic substitution NM_001165963. 4(*SCN1A*):c.4002 + 2461 T > C (Table 2, Fig. 1) has been demonstrated by minigene assays to induce the exonization of an out-of-frame 64-bp intronic sequence [17]. This 64-bp exonization mechanism has not been elucidated, but was correctly identified by SpliceAI with low DS (AG: 0.18; DG: 0.15). Using SpliceAI-visual, we show that while the DS are below the recommended threshold, the RS for the wild-type sequence are already significant (acceptor site: 0.64; donor site: 0.73). This results in high RS for the variant sequence T > C (acceptor site: 0.82; donor site: 0.87) and finally in the inclusion of the intronic sequence in the transcript. The mRNA proportion aberrant/normal transcript was not estimated.

MFGE8 Similarly, the pathogenic variant NM_005928.4(*MFGE8*):c.871-803A > G is responsible for the inclusion of an intronic sequence containing a stop codon (Table 2, Fig. 2) [18]. Again, the SpliceAI DS are low (AG: 0.15; DG: 0.16), but the reference allele was already identified with mild RS.

SpliceAI-visual identified the resulting acceptor and donor sites on the variant allele as strong candidates (respectively, 0.84 and 0.74), and the use of a graphical output (bedGraph files) loaded in a genome browser allowed a quick identification of the termination codon using the three frames translation track in IGV or in the UCSC Genome Browser. This intronic inclusion was estimated to be ~ 10 times more abundant than the wild-type transcript.

Unpublished cases

SETD5: enhancing the retention of a "poison" exon

Genome-trio sequencing of patient 1 revealed a de novo variant in intron 17 of *SETD5*: NM_001080517.3:c.2 476 + 198A > C (Table 2, Fig. 3). SpliceAI DS were low with an AG and DG of 0.05 and 0.04, respectively. However, those DS were added to high RS (acceptor: 0.94, donor: 0.95) as shown by SpliceAI-visual. Indeed, we observed a low level of intronic retention in RNAseq of controls. This intronic retention of 97 bp led to the inclusion of a premature stop codon and a presumed degradation by NMD. By performing RNAseq from a blood sample of the patient, we showed that the intronic retention of this "poison" exon was dramatically enhanced compared to 2 controls. The variant was found in 95% of the reads, confirming the causal effect of our variant on this retention. *GRN: guiding functional investigations* SpliceAIvisual is also convenient for guiding functional investigations. The following heterozygous variant NM_002087.4(*GRN*):c.-9A > G (Table 2) was identified in a 70-year-old male with Fronto-Temporal Dementia (patient 2), and plasmatic progranulin values compatible with a monoallelic alteration of *GRN* (see Sup Methods and Patients). This variant was previously identified in another affected patient, but the authors failed to evidence any abnormal splicing products [19]. This variant is predicted by SpliceAI to weaken the canonical donor site of this first 5'UTR exon (donor loss of 0.48). The initial RT-PCR has been performed on fibroblasts, but the exonic primers (F1-R1) failed to identify any abnormal products, as previously reported, even in the presence of an NMD inhibitor. Thanks to SpliceAI-visual, we were able to spot the putative rescuing donor site, which was predicted with a modest gain of + 0.19, but added to an RS of 0.75 on the reference allele (Fig. 4). This prediction was in favor of a 271-bp intronic retention. Another reverse primer (R2) has been designed in the predicted intronic 271-bp retention and showed amplification in the patient, and not in control individuals. The failure of the initial exonic RT-PCR (F1-R1) to amplify both wild-type and retention fragments could be due to the competitive advantage of the short fragment over the fragment including the 271-bp retention.

Adjusting the PVS1 criteria

According to the standard guidelines of the American College of Medical Genetics and Genomics (ACMG), the PVS1 criteria includes "canonical +/− 1 or 2 splice sites in a gene where the loss of function is a known mechanism of disease" [21]. However, alteration of a canonical splice site can result in other non-truncating consequences by various mechanisms: (1) an in-frame exon skipping (initially stated in the caveats of the aforementioned guideline), (2) an in-frame deletion by the creation of an exonic rescuing splice site, or (3) an in frame intronic retention devoid of in-frame stop codon [22, 23]. We show here with various cases the relevance of SpliceAI-visual in the assessment of the PVS1 criteria relative to variants altering canonical splice sites.

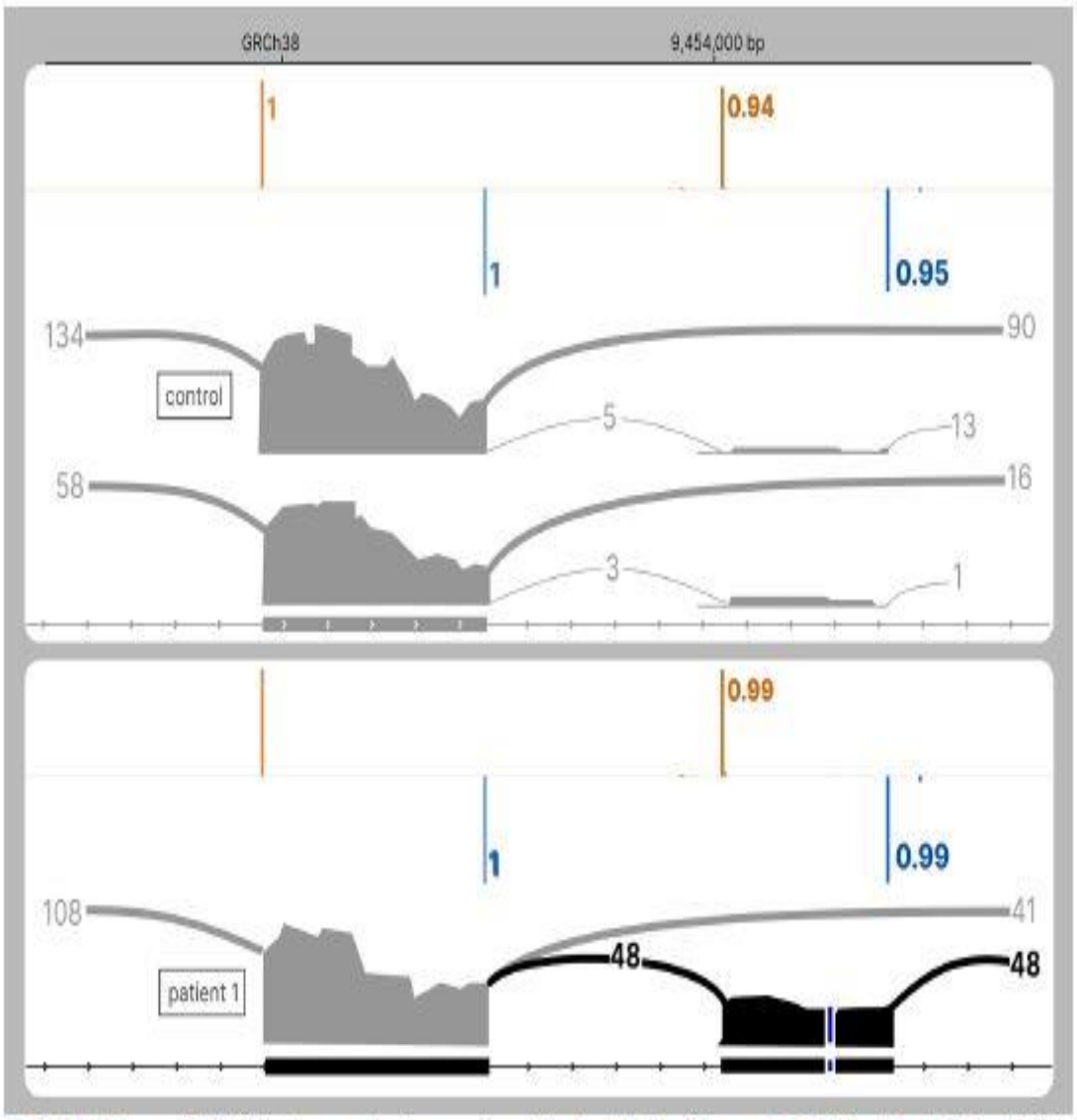

Fig. 3 The delta score pitfall: *SETD5* poison exon retention caused by an intronic substitution. RNAseq and SpliceAI-visual outputs displayed in IGV. Above: SpliceAI RS for the reference allele of *SETD5*, along with one control individual; below: SpliceAI RS for the pathogenic deep intronic variant NM_001080517.3:c.2476 + 198A > C, along with RNAseq of patient 1. Orange: acceptor site prediction; Blue: donor site prediction. The variant position is pointed out with a dashed line. Although the variant A > C is heterozygous, 95% of RNAseq reads carry the C, suggesting the causative role of this allele in the retention

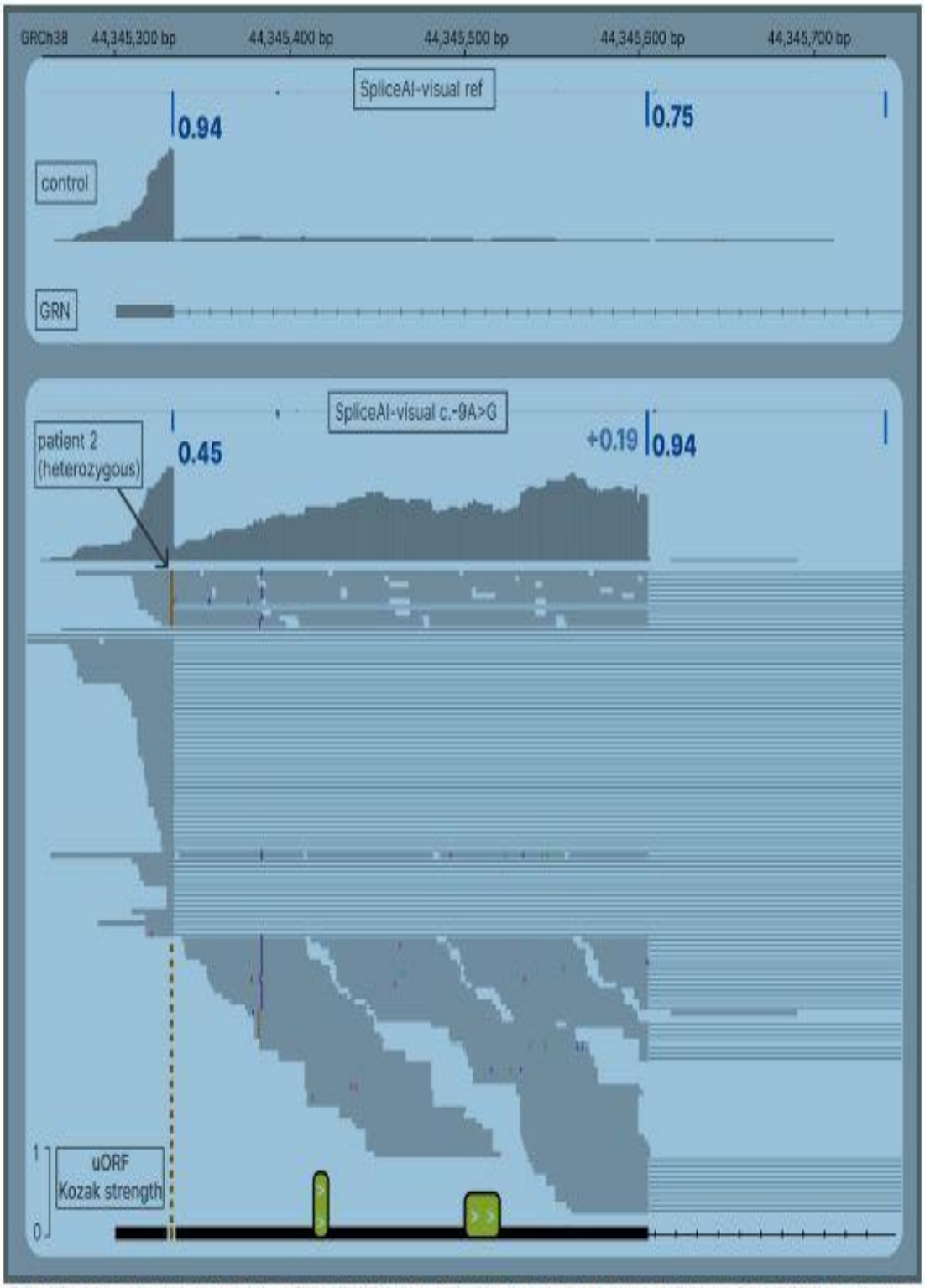

Fig. 4 The delta score pitfall: extending the 5'UTR of *GRN*. RNAseq and SpliceAI-visual outputs displayed in IGV. Above: SpliceAI RS for the reference allele of *GRN* along with RNAseq from one control; below: SpliceAI RS for NM_002087.4(*GRN*):c.-9A > G, along with RNAseq of patient 2. Bottom: two upstream Open Reading Frames in the intronic retention (yellow), height corresponding to the initiation strength of the AUG codon based on the Kozak context from TIS [20]

CASK We report the case of a 9-year-old male individual, presenting with learning disabilities and microcephaly (see Additional file 1: Methods and Patients, patient 3). Solo-exome sequencing showed a hemizygous substitution in a canonical donor site of the gene *CASK*, NM_003688.3(*CASK*):c.172 + 1G > A, absent from control databases (gnomAD, deCAF) [24, 25]. No other pathogenic or likely pathogenic variant was retained. This donor site disruption affects the MANE transcript of *CASK*. This hemizygous variant of patient 3 is predicted by SpliceAI to result in a DL, along with a + 0.71 DG. With SpliceAI-visual, this DG was predicted to lead to in-frame retention of 18 bp (6 amino acids, no stop codon, Fig. 5). Furthermore, this donor's DS of + 0.71 adds to a probability of 0.28 on the reference allele, resulting in an RS of 0.99 on this donor site (Fig. 5). In accordance with SpliceAI-visual predictions, RT-PCR on peripheral blood of patient 3 identified the 18-bp retention on 100% of transcripts (Fig. 5), which precluded the use of the Very_Strong weight of the PVS1 criteria. Without the very strong weight, this variant couldn't be classified as likely pathogenic or pathogenic. The significance of this variant was classified as Uncertain (Table 2).

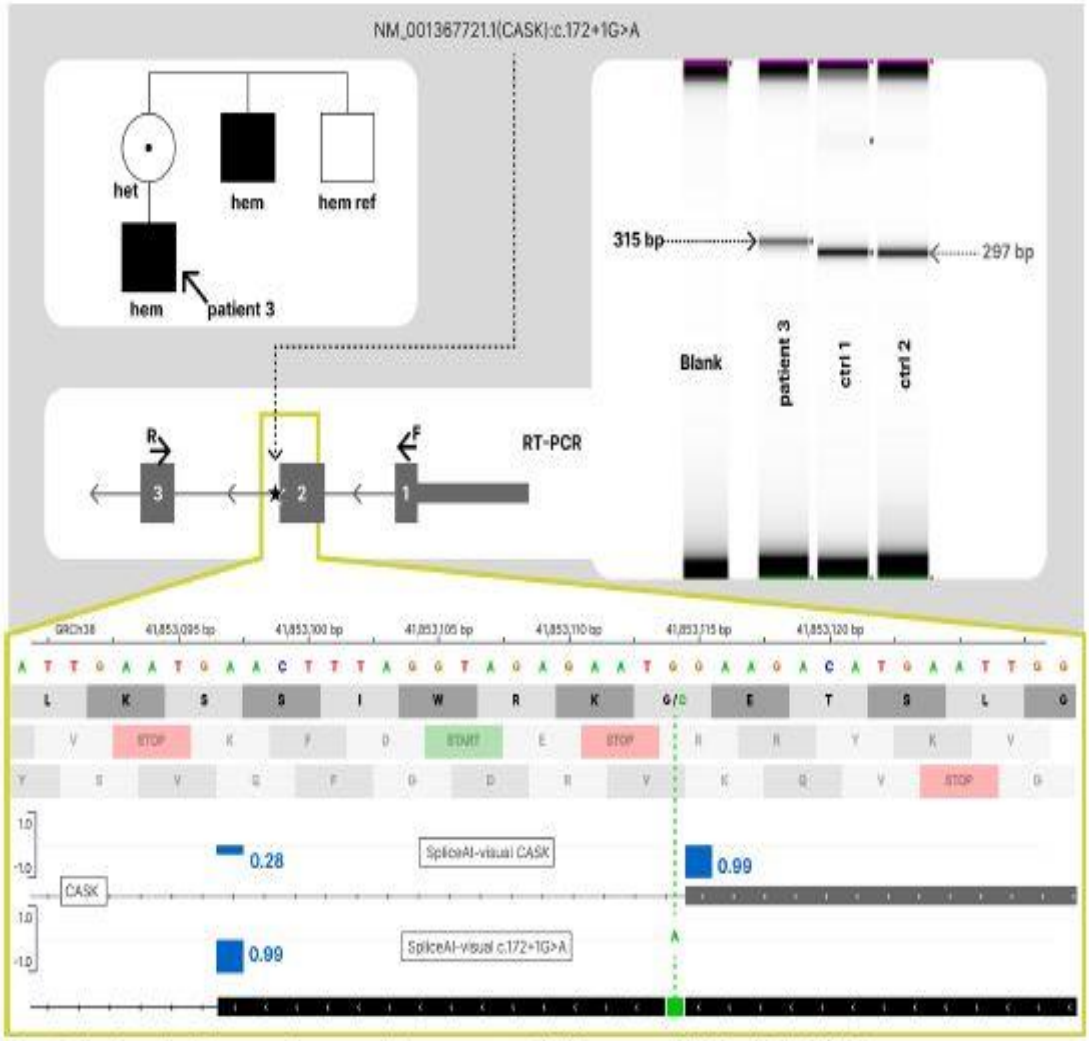

Fig. 5 Scaling down the PVS1 criteria of a canonical splice site variant in *CASK* Segregation, RT-PCR and SpliceAI RS of NM_003688.3(*CASK*):c.172 + 1G > A, hemizygous in patient 3. This variant leads to the complete in-frame retention of 18 bp (no wild-type 297 bp product was observed in patient 3 RT-PCR lane), as predicted by SpliceAI-visual. This 18-bp retention does not include stop codon and is predicted to insert 6 amino acids

KMT2D The variants NM_003482.4(*KMT2D*):c.5189- 1G > C and c.5782 + 1G > A (Table 2) are located in canonical splice sites of *KMT2D* and solely on this argument, the PVS1 criteria could apply, as loss-of-function variants are a known mechanism of *KMT2D*-related Kabuki syndrome. Based on this argument, these variants have recently been submitted as Likely Pathogenic in ClinVar (VCV001496460.1, VCV001506261.1) [26]. Surprisingly, these variants were reported in unaffected individuals in the general population (c.5189- 1G > C is absent from gnomAD v2.1.1 / v3.1.2, but found in 11 individuals in UK Biobank exomes [24, 27]. c.5782 + 1G > A is present in 3 heterozygous individuals in gnomAD v2 and v3) [24], which is inconsistent with the penetrance and severity of monoallelic *KMT2D* lossof-function variants (OMIM: 147,920). This discrepancy could be explained by splicing rescue, which was well predicted by SpliceAI-visual (Fig. 6).

• For c.5189-1G > C, SpliceAI-visual shows the creation of an in-frame rescuing acceptor site, predicted to delete 8 poorly conserved residues.

• For c.5782 + 1G > A, SpliceAI-visual predicts the complete loss of the donor site (− 1), and a modest gain of an in-frame nearby donor site (+ 0.28). This modest gain is another example of the DS pitfall (see above), adding on to a cryptic site predicted with an RS of 0.71 on the reference allele, resulting in an RS of 0.99 on the alternate allele. Moreover, this donor rescuing site results theoretically in the inclusion of 3 amino acids in the final product, which may have less deleterious consequences and explain the presence of this variant in gnomAD.

Fig. 6 Scaling down the PVS1 criteria of canonical splice site variants in *KMT2D*. Left: another a priori PVS1 variant NM_003482.4(*KMT2D*):c.5189-1G > C, present in 11 individuals in UK Biobank. This variant is predicted to result in an in-frame rescuing acceptor site, deleting 8 poorly conserved amino acids. Right: SpliceAI-visual outputs and BAM from one heterozygous from gnomAD of NM_003482.4(*KMT2D*):c.5782 + 1G > A. This variant is present in 3 individuals in gnomAD, which is not consistent with the penetrance of loss-of-function variants of *KMT2D*. Also, the mild rescuing DS of 0.28 is added to a nonzero RS on the reference allele (delta score pitfall) and is predicted to result in a complete rescue of this donor site, with the in-frame retention of 9 bp

For c.5189-1G > C, SpliceAI-visual shows the creation of an in-frame rescuing acceptor site, predicted to delete 8 poorly conserved residues. For c.5782 + 1G > A, SpliceAI-visual predicts the complete loss of the donor site (− 1), and a modest gain of an in-frame nearby donor site (+ 0.28). This modest gain is another example of the DS pitfall (see above), adding

on to a cryptic site predicted with an RS of 0.71 on the reference allele, resulting in an RS of 0.99 on the alternate allele. Moreover, this donor-rescuing site results theoretically in the inclusion of 3 amino acids in the final product, which may have less deleterious consequences and explain the presence of this variant in gnomAD.

TTN We describe here a similar case occurring in the *TTN* gene. NGS analyses targeted on congenital myopathy and muscular dystrophy gene panels identified in patient 4 (see Suppl. Methods for the phenotypic description) a variant in intron 116 of *TTN*: NM_001267550: c.31439-1G > C (Table 2) absent in the general population (gnomAD, deCAF) [24, 25] and predicted to affect splicing in exon 117. This variant located in the exon/intron junction of exon 117 is predicted to completely abolish the natural acceptor site, whereas the graphical output of SpliceAIvisual clearly shows a cryptic acceptor site located 9-bp downstream of the natural site (Fig. 7). Its use would lead to a 9-bp in-frame loss in exon 117, which has been confirmed by the RNAseq experiments (77 reads supporting the cryptic junction out of 222 reads (34.6%). Interestingly, SpliceAI-visual reveals a non-total raw probability of 0.53 to this rescuing acceptor site. Moreover, SpliceAI predicts the reduced strength of the natural donor site, located on the other side of exon 117. Taken together, these elements suggest a partial skipping of exon 117, which is further supported experimentally, as the exon 116–118 junction is attested by one read on RNAseq, and not seen in the two controls (Fig. 7). In the absence of a parental segregation study (no parents available) for dominant hypothesis, and of a second identified variant for recessive hypothesis, and regarding the RNAseq results, this variant was classified as a variant of uncertain significance (class 3).

SETD5 The following variant in *SETD5* was identified in patient 5 in the heterozygous state, NM_001080517.3(*SETD5*) : c .568-31_568dup p.(Asn190IlefsTer20) (Table 2), inherited from his asymptomatic mother. This 31-bp duplication is absent from gnomAD or deCAF [24, 25]; it duplicates the exon– intron border of exon 8 of *SETD5* and is considered to have a high truncating impact according to SNPEff and VEP annotators [28, 29]. Indeed, this variant duplicates the acceptor site, resulting in two competing nearby acceptor sites: the first being out-of-frame—hence the predicted frameshift—and the second being in-frame. SpliceAI-visual, however, shows the second site to be the strongest, predicting no splicing alteration (Fig. 8), which was confirmed by RNAseq.

Interpreting complex delins

Finally, SpliceAI-visual allows the interpretation of complex variants. For example, the following variant is a complex deletion–insertion variant occurring on an exon–intron border in the gene NM_001142800.2(*EY S*):c.2992_2992 + 6delinsTG (Table 2). However, most SpliceAI current public implementations or pre-computed whole genome VCFs currently do not process complex delins variations (i.e., other than deletion, insertion, or substitution), nor does Pangolin. Of note, those complex variations are handled by CI-SpliceAI but with numerical results [12]. The functional study of this variant by a minigene assay has shown the skipping of an entire out-of-frame exon [30]. We show that this exon skipping is well predicted by SpliceAI-visual (Fig. 9). In addition, we have tested SpliceAI-visual's ability to predict 13 other complex delins, all of which were functionally attested to alter splicing, and correctly predicted by SpliceAI-visual (Additional file 1: Table S1).

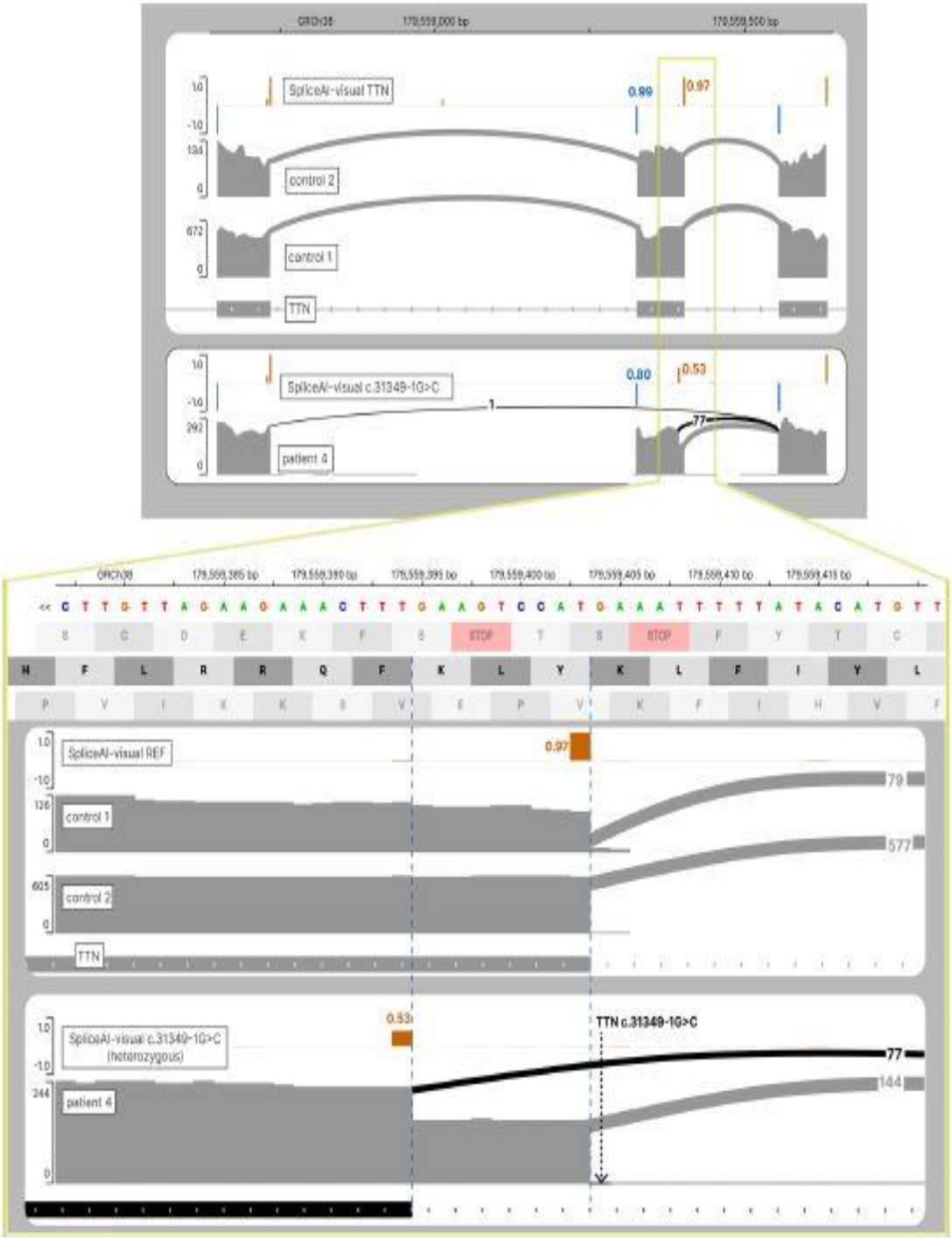

Fig. 7 Scaling down the PVS1 criteria of a canonical splice site variant in *TTN*. RNAseq and SpliceAI-visual outputs displayed in IGV showing the predicted exon skipping (top view), and the in-frame rescue (bottom view). Top tracks: SpliceAI RS for the reference allele of *TTN* along with RNAseq from 2 controls; bottom tracks: SpliceAI RS for the NM_001267550.2(*TTN*):c.31349-1G > C along with RNAseq of patient 4

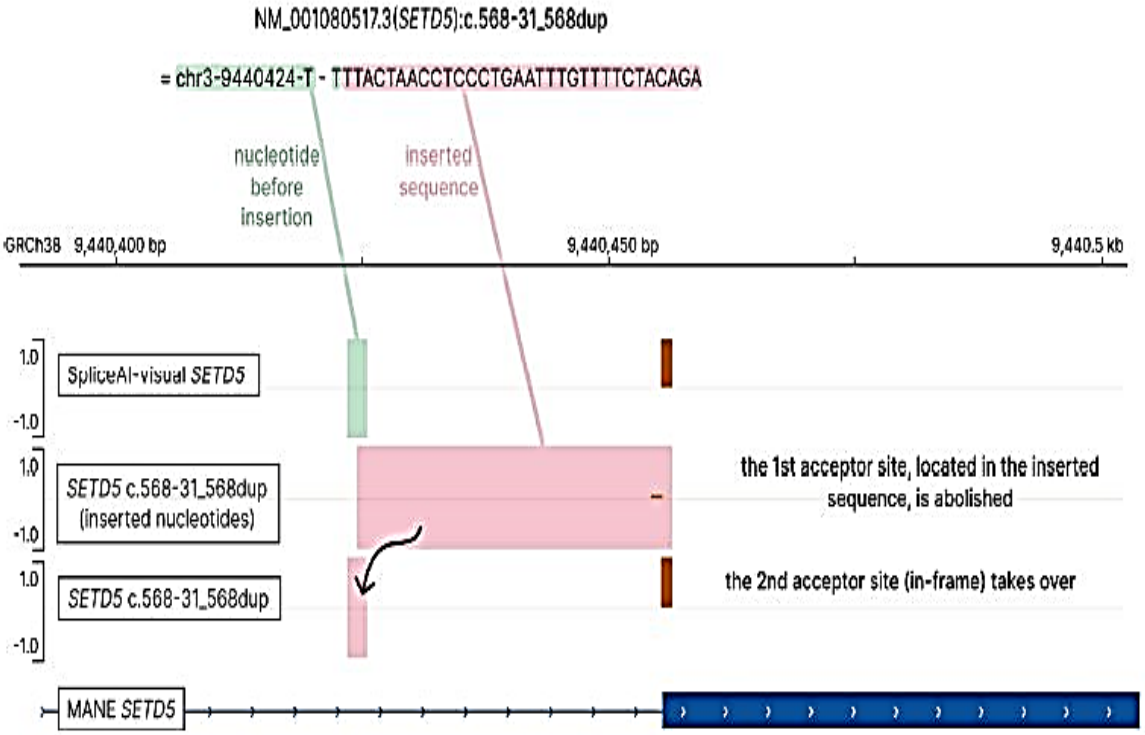

Fig. 8 Scaling down the PVS1 criteria of a putative frameshift in *SETD5*. SpliceAI-visual outputs displayed in IGV showing the predicted benign splicing outcome of this putative frameshift

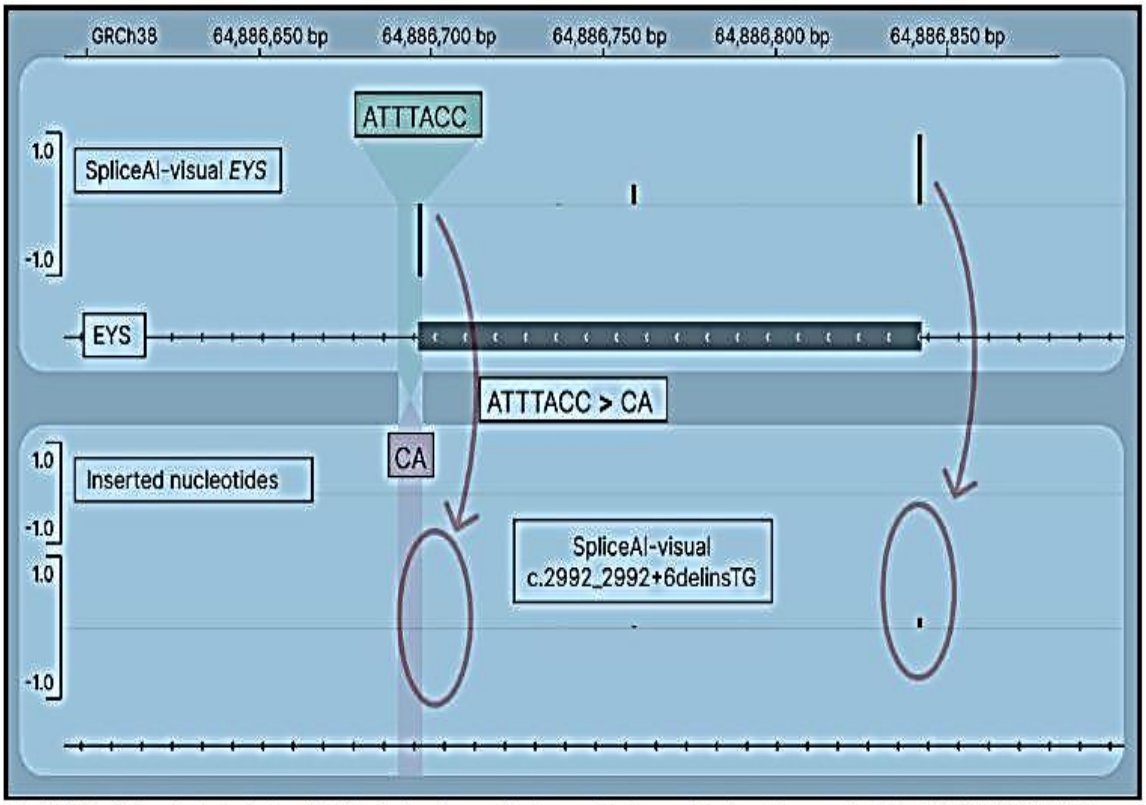

Fig. 9 SpliceAI-visual outputs displayed in IGV showing the predicted exon skipping resulting from the complex delins NM_001142800.2(*EYS*): c.2992_2992+6delinsTG. Top track: SpliceAI RS for the reference allele of *EYS*; bottom track: SpliceAI RS for the delins in *EYS*

Discussion

Functional validation of putative splice-altering variants is often difficult and resource-consuming. Also, besides their accessibility, specific RT-PCR, RNA sequencing or minigene assays all have their limitations (e.g., primer design, tissue expression, restricted to middle exon, etc.4). Given the growing number of putative splice-altering variants identified by large genome sequencing, the decision to perform such functional splicing assays is not trivial. The relevance of prediction tools to filter and to accurately evaluate a variant's expected splicing outcome is crucial.

We have shown that the DS of SpliceAI's predictions could in certain cases be misleading, and have introduced the relevance of interpreting splicing predictions with RS, as a complementary analysis. The threshold of 0.20 used for DS has been qualified as "relatively permissive" and as a "high recall" threshold by the original authors of SpliceAI (https:// github. com/Illum ina/ Splic eAI).2 However, the three deep intronic pathogenic or likely pathogenic splicing variants of *SCN1A*, *MFGE8*, and *SETD5* would have been filtered out with this threshold. SpliceAI-visual represents a convenient manner to predict the splicing outcomes of these variants.

Interestingly, the authors of SpliceAI observed a decreased sensitivity of SpliceAI to predict the splice alterations of deep intronic variants, compared to variants located near exons. This was also recently reported for Pangolin [11]. They hypothesized this phenomenon to be caused by a putative intronic deprivation of specific markers, which are usually enriched near exons by selection. This diminished performance of SpliceAI in deep introns could also be partly explained by the pitfall of the DS approach. A recent study has shown a depletion of competitive decoy donors near the exon–intron junction [31]. If we hypothesize this donor site depletion to similarly affect acceptor sites, it is easy to think of introns as enriched of such dormant cryptic splice sites, as shown in Fig. 1. These cryptic intronic sites would be detected by SpliceAI, with non-null value in the reference allele, introducing an intronic bias for higher reference allele scores, and lower DS.

The need to access SpliceAI RS has been manifested in a recent study, aimed at predicting the activation of donor cryptic sites by a variant [31]. In line with this study, we believe that special caution should be taken into consideration when assessing the PVS1 criteria related to canonical position splicing outcomes. Indeed, splice alterations at these positions may lead to consequences differing significantly from a truncating variant, meaning typically in-frame insertion of a few nucleotides [22, 23, 32].

Concerning patient 3, according to the ACMG guidelines, the variant NM_003688.3(*CASK*):c.172 + 1G > A meets a priori the loss-of-function criteria (PVS1). However, patient 3 presented only a mild intellectual disability (see Patients and Methods), in striking contrast to the other patients reported with *CASK* loss-of-function variants. To our knowledge, only female patients have been reported with loss-of-function variants in *CASK*, all with severe developmental delay. Some male patients have been reported with truncating variants, but they were mosaic [33, 34]. Interestingly, four affected males were reported with a canonical acceptor site NM_001367721.1(*CASK*):c.2521-2A > T along with a mild phenotype. RT-PCR showed two in-frame deletions (an in-frame exon skipping—28 amino acids—and a 3 amino acid deletion), inconsistent with the lossof- function criteria, PVS1 [35]. Of note, both of these in-frame deletions were predicted by SpliceAI-visual. We decided

not to apply the PVS1 criteria for NM_0 03688.3(*CASK*):c.172 + 1G > A in patient 3, based on the RT-PCR amplification of the predicted 18-bp retention. In addition, NM_003688.3(*CASK*):c.172 + 1G > A was inherited from the asymptomatic mother, found at the hemizygous state in one symptomatic uncle with learning disabilities and absent from another asymptomatic uncle. This variant is currently classified as VUS, although it cannot be ruled out that this insertion of 6 amino acids is mildly deleterious at the hemizygous state, which would be consistent with the four affected males previously reported, along with the familial segregation analysis.

Using SpliceAI-visual when interpreting variants at canonical splice sites may avoid potential misinterpretation of their consequences, and allow correct prediction of the effect at the RNA level. Of course, the functional validation of the predicted effect remains necessary; however, if an in-frame consequence is clearly expected by SpliceAI and SpliceAI-visual, we propose to modulate the weight associated with the PVS1 criteria, following ClinGen Sequence Variant Interpretation Workgroup [36](p1). In addition to variants at canonical splice sites, the strength of the PVS1 criteria may also be modulated for predicted PTCs. Indeed, many putative PTCs have been reported to impact splicing, with in-frame consequences, associated with milder, or partial rescue of the associated phenotype [22, 23, 32, 37, 38].

Monoallelic alterations of the *SETD5* gene are implicated in intellectual disability, combining delayed psychomotor development and poor language development (OMIM #615761). The duplication of a natural splice site in *SETD5* identified in patient 5 in the heterozygous state, absent from the gnomAD database, and annotated as frameshift would have been consistent with the previous descriptions, where the intellectual disability is often mild. This variant was inherited from the asymptomatic mother, but this has been previously described for other pathogenic *SETD5* variants [39]. Thanks to SpliceAI-visual, the benign splicing outcome of this was further confirmed by RNAseq. The variant was then assumed to be probably benign.

SpliceAI-visual has also been useful to guide functional exploration in the *GRN* case, as it enabled the correct design of RT-PCR primers specific to the intronic retention. *GRN* RNAseq was consistent with monoallelic retention. Indeed, the exonic heterozygous c.-9A > G is only supported by reads aligned in the intronic retention, suggesting a total effect on splicing. Indeed, the low allele fraction observed on the sequence reads is presumably due to the 3' bias of polyA mRNAseq, according to which the depth of the coverage decreases as the distance from the polyA tail increases. As the mRNA carrying the variant is shifted 271 bp after the intronic retention, it is more distant from the polyA than the wild-type mRNA at the position of the variant. As a consequence, this 271-bp difference in distance from the polyA results in a deeper coverage of the wild-type mRNA, relative to the mutated mRNA at the variant site. As to the mechanism by which this 271-bp intronic retention leads to a reduced amount of PGRN, we propose the following hypothesis. As previously described, the amount of transcript has been found to be similar in the presence or in the absence of nonsense-mediated decay (NMD) inhibitor, suggesting a limited NMD effect [19]. Interestingly, the retention included two AUG codons with moderate potential to initiate translation, as their Kozak consensus sequence strength was similar to that of the natural AUG of *GRN*. As small upstream open reading frames (uORF) can reduce the translation efficiency of a transcript, we hypothesize that these uORFs caused a nearly complete extinction of translation in the transcript including the retention [40].

SpliceAI-visual is also useful to assess the splicing outcomes of complex variants such as deletions/ insertions, as, apart from running a private instance of SpliceAI, this is currently the

only tool that computes such SpliceAI predictions. Such "complex" deletions/ insertions are not rare (7387 of such variants in clinvar, accessed 2022/07/03) [26] and often lack decent tools to be correctly assessed. Thanks to SpliceAI-visual, their splicing outcome can now be predicted. Similarly, the analysis of very large size variants, like Copy Number Variants, Inversions, and Mobile Element Insertion, can be achieved with SpliceAI-visual's Colab version. The only size limitation would be the limits of the transcript. Taken together, although SpliceAI's numerical DS are convenient for batch filtering, and powerful in many cases, we expose here some limitations when it comes to the careful examination of a variation in human pathology. We show the advantages of the SpliceAIvisual graphical output, RS approach to interpret splice-altering candidate variants, and we believe both tools to be complementary in the daily practice of medical genetics.

Acknowledgements

The authors gratefully thank all the patients and parents involved in this work.

Author contributions

DB and J-MSA contributed to conceptualization; DB, BC, J-MSA, and PG curated the data; AP, EL, LF, TB, MF, JB, FC, FP, BI, CV, CVG, JR, and MM investigated the study; DB and J-MSA contributed to software; DB and J-MSA visualized the study; J-MSA contributed to writing—original draft; DB, BC, J-MSA, AB, MC, VK, A-FR, PG, AP, and ELG contributed to writing—review and editing. All authors read and approved the final manuscript.

Funding

This work was funded by AFM Grant 21384 (The French Muscular Dystrophy Association (AFM-Telethon)) and the Delegation a la Recherche Clinique et a l'Innovation du Groupement de Cooperation Sanitaire de la Mission d'Enseignement, de Recherche, de Reference et d'Innovation (DRCI-GCSMERRI) de Montpellier-Nimes.

Availability of data and materials

SpliceAI-visual is freely available on MobiDetails at https:// mobid etails. iurc.montp. inserm. fr/ MD/, or in Google Colaboratory at https:// tinyu rl. com/ spliceai-visual. It can be freely copied for local usage, or used online in Google Colaboratory with the requirement of a Google account. All variants described in this manuscript are available in MobiDetails (https:// mobid etails. iurc. montp.inserm. fr/ MD/ auth/ varia nt_ list/ splic eAI_ visual_ 2022 or https:// tinyu rl. com/bpyz9 x6j). Variants included in the Additional file 1: Table S1 are also available in MobiDetails (https:// mobid etails. iurc. montp. inserm. fr/ MD/ auth/ varia nt_ list/splic eAI_ visual_ compl ex_ 2022or https:// tinyu rl. com/ 49nuj ud4). MobiDetails code is available at https:// github. com/ beboc he/ MobiD etails and the SpliceAI REST API code designed for this work at https:// github. com/ mobid ic/ splic eai.

Declarations

Ethics approval and consent to participate

A written informed consent was obtained from all participants as required by the guidelines of the Declaration of Helsinki, and approved on April, 8, 2019, by the Research Ethics Committee of Brest (IDRCB: 2018-A02287-48).

Competing interests

The authors declare that they have no competing interests.

References

1. Lopez-Bigas N, Audit B, Ouzounis C, Parra G, Guigo R. Are splicing mutations the most frequent cause of hereditary disease? FEBS Lett. 2005;579(9):1900–3. https:// doi. org/ 10. 1016/j. febsl et. 2005. 02. 047.

2. Jaganathan K, Kyriazopoulou Panagiotopoulou S, McRae JF, et al. Predicting splicing from primary sequence with deep learning. Cell. 2019;176(3):535-548.e24. https:// doi. org/ 10. 1016/j. cell. 2018. 12. 015.

3. Wai HA, Lord J, Lyon M, et al. Blood RNA analysis can increase clinical diagnostic rate and resolve variants of uncertain significance. Genet Med. 2020;22(6):1005–14. https:// doi. org/ 10. 1038/ s41436-020-0766-9.

4. Ha C, Kim JW, Jang JH. Performance evaluation of SpliceAI for the prediction of splicing of NF1 variants. Genes. 2021;12(9):1308. https:// doi. org/10. 3390/ genes 12091 308.

5. Bychkov I, Galushkin A, Filatova A, et al. Functional analysis of the PCCA and PCCB gene variants predicted to affect splicing. IJMS. 2021;22(8):4154. https:// doi. org/ 10. 3390/ ijms2 20841 54.

6. Danis D, Jacobsen JOB, Carmody LC, et al. Interpretable prioritization of splice variants in diagnostic next-generation sequencing. Am J Hum Genet. 2021;108(9):1564–77. https:// doi. org/ 10. 1016/j. ajhg. 2021. 06. 014.

7. Dawes R, Joshi H, Cooper ST. Empirical prediction of variant-activated cryptic splice donors using population-based RNA-Seq data. Nat Commun. 2022;13(1):1655. https:// doi. org/ 10. 1038/ s41467-022-29271-y.

8. Rowlands C, Thomas HB, Lord J, et al. Comparison of in silico strategies to prioritize rare genomic variants impacting RNA splicing for the diagnosis of genomic disorders. Sci Rep. 2021;11(1):20607. https:// doi. org/ 10. 1038/s41598-021-99747-2.

9. Bournazos AM, Riley LG, Bommireddipalli S, et al. Standardized practices for RNA diagnostics using clinically accessible specimens reclassifies 75% of putative splicing variants. Genet Med. 2022;24(1):130–45. https:// doi.org/ 10. 1016/j. gim. 2021. 09. 001.

10. Li K, Luo T, Zhu Y, et al. Performance evaluation of differential splicing analysis methods and splicing analytics platform construction. Nucleic Acids Res. 2022;50(16):9115–26. https:// doi. org/ 10. 1093/ nar/ gkac6 86.

11. Zeng T, Li YI. Predicting RNA splicing from DNA sequence using Pangolin. Genome Biol. 2022;23(1):103. https:// doi. org/ 10. 1186/s13059-022-02664-4.

12. Strauch Y, Lord J, Niranjan M, Baralle D. CI-SpliceAI-Improving machine learning predictions of disease causing splicing variants using curated alternative splice sites. PLoS ONE. 2022;17(6):e0269159. https:// doi. org/10. 1371/ journ al. pone. 02691 59.

13. Kent WJ, Sugnet CW, Furey TS, et al. The human genome browser at UCSC. Genome Res. 2002;12(6):996–1006. https:// doi. org/ 10. 1101/ gr.229102.

14. Robinson JT, Thorvaldsdottir H, Wenger AM, Zehir A, Mesirov JP. Variant review with the integrative genomics viewer. Cancer Res. 2017;77(21):e31–4. https:// doi. org/ 10. 1158/ 0008-5472. CAN-17-0337.

15. Baux D, Van Goethem C, Ardouin O, et al. MobiDetails: online DNA variants interpretation. Eur J Hum Genet. 2021;29(2):356–60. https:// doi. org/10. 1038/ s41431-020-00755-z.

16. Morales J, Pujar S, Loveland JE, et al. A joint NCBI and EMBL-EBI transcript set for clinical genomics and research. Nature. 2022;604(7905):310–5. https:// doi. org/ 10. 1038/ s41586-022-04558-8.

17. Li Q, Wang Y, Pan Y, Wang J, Yu W, Wang X. Unraveling synonymous and deep intronic variants causing aberrant splicing in two genetically undiagnosed epilepsy families. BMC Med Genom. 2021;14(1):152. https:// doi.org/ 10. 1186/ s12920-021-01008-8.

18. Yamaguchi H, Fujimoto T, Nakamura S, et al. Aberrant splicing of the milk fat globule-EGF factor 8 (MFG-E8) gene in human systemic lupus erythematosus. Eur J Immunol. 2010;40(6):1778–85. https:// doi. org/ 10. 1002/ eji.20094 0096.

19. Puoti G, Lerza MC, Ferretti MG, Bugiani O, Tagliavini F, Rossi G. A mutation in the 5'-UTR of GRN gene associated with frontotemporal lobar degeneration: phenotypic variability and possible pathogenetic mechanisms. J Alzheimers Dis. 2014;42(3):939–47. https:// doi. org/ 10. 3233/ JAD-140717.

20. Gleason AC, Ghadge G, Chen J, Sonobe Y, Roos RP. Machine learning predicts translation initiation sites in neurologic diseases with nucleotide repeat expansions. PLoS ONE. 2022;17(6):e0256411. https:// doi. org/ 10. 1371/ journ al. pone. 02564 11.

21. on behalf of the ACMG Laboratory Quality Assurance Committee, Richards S, Aziz N, et al. Standards and guidelines for the interpretation of sequence variants: a joint consensus recommendation of the American College of Medical Genetics and Genomics and the Association for Molecular Pathology. Genet Med. 2015;17(5):405–423. https:// doi. org/ 10. 1038/ gim. 2015. 30.

22. Mesman RLS, Calleja FMGR, de la Hoya M, et al. Alternative mRNA splicing can attenuate the pathogenicity of presumed loss-of-function variants in BRCA2. Genet Med. 2020;22(8):1355–65. https:// doi. org/ 10. 1038/s41436-020-0814-5.

23. Hinzpeter A, Aissat A, Sondo E, et al. Alternative splicing at a NAGNAG acceptor site as a novel phenotype modifier. PLoS Genet. 2010;6(10):e1001153. https:// doi. org/ 10. 1371/ journ al. pgen. 10011 53.

24. Genome Aggregation Database Consortium, Karczewski KJ, Francioli LC, et al. The mutational constraint spectrum quantified from variation in 141,456 humans. Nature. 2020;581(7809):434–443. https:// doi. org/ 10.1038/ s41586-020-2308-7

25. Halldorsson BV, Eggertsson HP, Moore KHS, et al. The sequences of 150,119 genomes in the UK Biobank. Nature. 2022;607(7920):732–40. https:// doi. org/ 10. 1038/ s41586-022-04965-x.

26. Landrum MJ, Lee JM, Benson M, et al. ClinVar: improving access to variant interpretations and supporting evidence. Nucleic Acids Res. 2018;46(D1):D1062–7. https:// doi. org/ 10. 1093/ nar/ gkx11 53.

27. Karczewski KJ, Solomonson M, Chao KR, et al. Systematic single-variant and gene-based association testing of thousands of phenotypes in 394,841 UK Biobank exomes. Cell Genom. 2022;2(9):100168. https:// doi.org/ 10. 1016/j. xgen. 2022. 100168.

28. Cingolani P, Platts A, Wang LL, et al. A program for annotating and predicting the effects of single nucleotide polymorphisms, SnpEff: SNPs in the genome of Drosophila melanogaster strain w1118; iso-2; iso-3. Fly (Austin). 2012;6(2):80–92. https:// doi. org/ 10. 4161/ fly. 19695.

29. McLaren W, Gil L, Hunt SE, et al. The ensembl variant effect predictor. Genome Biol. 2016;17(1):122. https:// doi. org/ 10. 1186/ s13059-016-0974-4.

30. Westin IM, Jonsson F, Osterman L, Holmberg M, Burstedt M, Golovleva I. EYS mutations and implementation of minigene assay for variant classification in EYS-associated retinitis pigmentosa in northern Sweden. Sci Rep. 2021;11(1):7696. https:// doi. org/ 10. 1038/ s41598-021-87224-9.

31. Dawes R, Joshi H, Cooper ST. Empirical prediction of variant-associated cryptic-donors with 87% sensitivity and 95% specificity. Genetics. 2021.https:// doi. org/ 10. 1101/ 2021. 07. 18. 452855.

32. Disset A, Bourgeois CF, Benmalek N, Claustres M, Stevenin J, Tuffery- Giraud S. An exon skipping-associated nonsense mutation in the dystrophin gene uncovers a complex interplay between multiple antagonistic splicing elements. Hum Mol Genet. 2006;15(6):999–1013. https:// doi. org/10. 1093/ hmg/ ddl015.

33. Burglen L, Chantot-Bastaraud S, Garel C, et al. Spectrum of pontocerebellar hypoplasia in 13 girls and boys with CASK mutations: confirmation patient. Orphanet J Rare Dis. 2012;7(1):18. https:// doi. org/ 10. 1186/1750-1172-7-18.

34. Moog U, Bierhals T, Brand K, et al. Phenotypic and molecular insights into CASK-related disorders in males. Orphanet J Rare Dis. 2015;10(1):44. https:// doi. org/ 10. 1186/ s13023-015-0256-3.

35. Hackett A, Tarpey PS, Licata A, et al. CASK mutations are frequent in males and cause X-linked nystagmus and variable XLMR phenotypes. Eur J Hum Genet. 2010;18(5):544–52. https:// doi. org/ 10. 1038/ ejhg. 2009. 220.

36. Abou Tayoun AN, Pesaran T, DiStefano MT, et al. Recommendations for interpreting the loss of function PVS1 ACMG/AMP variant criterion. Hum Mutat. 2018;39(11):1517–24. https:// doi. org/ 10. 1002/ humu. 23626.

37. Flanigan KM, Dunn DM, von Niederhausern A, et al. Nonsense mutation associated Becker muscular dystrophy: interplay between exon definition and splicing regulatory elements within the DMD gene. Hum Mutat. 2011;32(3):299–308. https:// doi. org/ 10. 1002/ humu. 21426.

38. Tuffery-Giraud S, Miro J, Koenig M, Claustres M. Normal and altered premRNA processing in the DMD gene. Hum Genet. 2017;136(9):1155–72. https:// doi. org/ 10. 1007/ s00439-017-1820-9.

39. Powis Z, Farwell Hagman KD, Mroske C, et al. Expansion and further delineation of the *SETD5* phenotype leading to global developmental delay, variable dysmorphic features, and reduced penetrance. Clin Genet. 2018;93(4):752–61. https:// doi. org/ 10. 1111/ cge. 13132.

40. Johnstone TG, Bazzini AA, Giraldez AJ. Upstream ORFs are prevalent translational repressors in vertebrates. EMBO J. 2016;35(7):706–23. https://doi. org/ 10. 15252/ embj. 20159 2759